Graphene-and-Copper Artificial Nacre Fabricated by a Preform Impregnation Process: Bioinspired Strategy for Strengthening-Toughening of Metal Matrix Composite

Ding-Bang Xiong, Mu Cao, Qiang Guo, Zhanqiu Tan, Genlian Fan, Zhiqiang Li,* and Di Zhang*

State Key Laboratory of Metal Matrix Composites, Shanghai Jiao Tong University, Shanghai 200240, China

ABSTRACT Metals can be strengthened by adding hard reinforcements, but such strategy usually compromises ductility and toughness. Natural nacre consists of hard and soft phases organized in a regular "brick-and-mortar" structure and exhibits a superior combination of mechanical strength and toughness, which is an attractive model for strengthening and toughening artificial composites, but such bioinspired metal matrix composite has yet to be made. Here we prepared nacre-like reduced graphene oxide (RGrO) reinforced Cu matrix composite based on a preform impregnation process, by which two-dimensional RGrO was used as "brick" and inserted into "□-and-mortar" ordered porous Cu preform (the symbol "□" means the absence of "brick"), followed by compacting. This process realized uniform dispersion and alignment of RGrO in Cu matrix simultaneously. The RGrO-and-Cu artificial nacres exhibited simultaneous enhancement on yield strength and ductility as well as increased modulus, attributed to RGrO strengthening, effective crack deflection and a possible combined failure mode of RGrO. The artificial nacres also showed significantly higher strengthening efficiency than other conventional Cu matrix composites, which might be related to the alignment of RGrO.

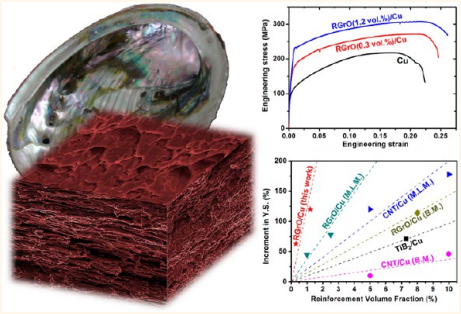

KEYWORDS: bioinspired strategy · artificial nacre · graphene · metal matrix composite · copper · strengthening and toughening

Metal matrix composites (MMCs) offer a rich and vast playground for extending the application range of metals, owing to their attractive combinations of mechanical properties and functionalities that are inaccessible to pure metals.[1,2] MMC usually has a higher strength than the metal matrix because of the addition of hard reinforcement, such as ceramic particle and carbon fiber, which is also the only approach to enhance the modulus of metal (capacity of resistance to elastic deformation that is determined by atomic bonds). But such strategy usually compromises ductility and toughness and results in catastrophic and unpredictable failure in applications, which has become the bottleneck of developing high performance MMCs.[3] How to design MMCs to achieve an optimum combination of strength and toughness is thus an ongoing and fascinating question.[4−6]

However, countless rigid biological materials exhibit a superior combination of strength and toughness and are used for structural purposes in nature.[7,8] The most famous example is probably the nacreous part of seashells. Nacre consists of 95 vol % of hard mineral aragonite (a polymorph of calcium carbonate) providing for strength, but nacre would be brittle without a means of dissipating strain, as the ductility and toughness reduction often seen in conventional MMCs with increasing the fraction of hard reinforcements. In fact, nacre presents a toughness (in energy terms) some 3 orders of magnitude greater than that of the main constituent aragonite because of a highly regular "brick-and-mortar" structure; the "bricks" are ∼200−900 nm thick, ∼5−8 μm wide, platelets of the mineral aragonite, bonded by protein mortar (∼10−50 nm thick) in-between.[5,7,8] The hard mineral

* Address correspondence to lizhq@sjtu.edu.cn, zhangdi@sjtu.edu.cn.

Received for review February 15, 2015 and accepted June 17, 2015.

Published online June 17, 2015
10.1021/acsnano.5b01067

aragonite accounts for the high strength, while the soft protein allows sliding of the aragonite platelets over each other through limited interlayer shearing, thereby conferring toughness. The structure–function harmony of nacre has inspired a large class of advanced inorganic/organic composites.[9,10] In MMCs, reinforcement is usually hard phase, while metal is ductile and can be considered as relatively soft phase. Therefore, mimicking the unique microstructure in natural nacre could be a reasonable strategy for enhancing strength without losing toughness or even simultaneously enhancing strength and toughness in MMCs, but such bioinspired MMC has yet to be made.

Nacre-inspired MMC could be achieved by building "brick-and-mortar" organized structures using high strength reinforcement with high aspect ratio as "brick" combined with ductile metal "mortar". While "brick" of reinforcement is by no means easy to obtain in processing artificial nacre, graphene (Gr) or reduced graphene oxide (RGrO) with its combination of inherent two-dimensional (2-D) sheet geometry (thin-brick-like) and outstanding mechanical properties shows great promise as an ideal candidate.[11] Actually, some success nacre-inspired examples about using graphene as "brick" have been reported in artificial polymer matrix composite.[12−14] We thereby select graphene as "brick" in fabricating nacre-inspired MMC.

Various techniques have been developed for fabricating nacre-inspired ceramic/polymer composites,[15] such as layer-by-layer,[16−18] ice templating,[19] electrophoretic deposition,[20] and vacuum evaporation and filtration,[14,21] but fabricating MMCs with a "brick-and-mortar" organized structure is still a great challenge. The major reasons lie in that homogeneous dispersion and alignment of reinforcement "brick" in metal matrix is difficult to be achieved by the techniques developed for nacre-inspired ceramic/polymer composites because of intrinsic differences between metal and polymer matrices, as well as some specific obstacles such as agglomeration of graphene, chemical reactions[22] and/or huge density discrepancy between graphene and metals. The sputtering[23] and ice-templating techniques[24] were applied to prepare ordered multilayered and laminated ceramic/metal composites. Although their alternated arrangements of ceramic and metal lamellae exhibited some similarities with natural nacre, the uninterrupted lamellae could not deflect crack (primary toughening mechanism in natural nacre) as effectively as a "brick-and-mortar" structure does.[19] Recently, a technique of flake powder metallurgy was established for fabricating metal matrix nanocomposites; nanoflake ductile metal powders covered with hard reinforcements were used as building blocks to be assembled together forming composites *via* compacting and extrusion.[25−27] Still, effective approach to fabricate desired nacre-inspired MMC in which separated nanoscale "bricks" of hard reinforcement are bonded by continuous ductile metal "mortar" has not been reported yet.

Here we propose a novel preform impregnation process to fabricate nacre-inspired MMC. RGrO was chosen as "brick" for its inherent 2-D geometry and superior mechanical properties. Cu was selected as representative metal for "mortar" because (1) it is widely used for structural as well as electrical and electronic purposes; (2) copper oxide impurities are easy to be reduced, making experimental system simple. Thanks to the bioinspired "brick-and-mortar" microstructure, the nacre-like RGrO reinforced Cu matrix composites exhibit simultaneous enhancement on strength and ductility as well as high strengthening efficiency, which offers an effective strategy for developing new high-performance MMCs.

RESULTS AND DISCUSSION

Preparation Strategy. The process we used here is based on a preform impregnation process, as illustrated in schematic diagram in Figure 1. The entire process consisted of three steps (Figure 1): replication of the ordered porous structure of fir wood with Cu, absorption of reduced graphene oxide into porous Cu preform, and a hot-pressed compacting. Fir wood has a highly ordered layered porous structure, in which pores are in rectangular shape with an average size of $\sim 20 \times 30\ \mu m$ and a wall thickness of $\sim 1.5\ \mu m$ (Figure 2a). The porous structure can be considered as parallel layers connected by staggered short walls, which is very similar to a "brick-and-mortar" structure but without "brick" because of the pores, namely a "□-and-mortar" structure. Afterward, we applied a chemical route including copper oxide replication and subsequent reduction to replicate the porous structure of fir wood with Cu, by which Cu preform with a "□-and-mortar" structure was obtained. The macro size of the as-replicated porous Cu preform depends on that of fir wood used, and a typical size of $2 \times 1.5 \times 1.5\ cm^3$ was prepared (Figure 2b). The replicated porous structure inherited that of fir wood very well, but with thinner wall thickness and slightly shrank pore size (Figure 2b). The wall is composed of Cu particles with size of hundreds nanometers and average wall thickness is about 500 nm (Figure 2b). According to the observed pore size and wall thickness, the porosity of the Cu preform is around 96%, which is consistent with the calculated relative density based on the measured macro size and weight, indicating that the uniformity of pores and homogeneity of replication.

With this "□-and-mortar" organized Cu preform, we can easily fabricate nacre-inspired MMC by simply inserting "brick" into the pores. RGrO was used as "brick" in this work. Homogeneous dispersing RGrO is extremely difficult in fabricating composites due to its 2-D atomic layer geometry, large surface area and high surface energy that easily lead to agglomerations, especially in strong and ductile metal matrices.[28]

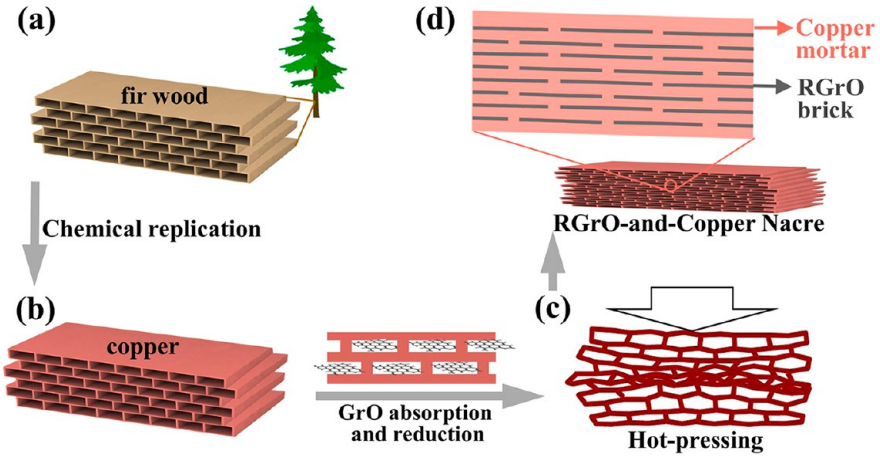

Figure 1. Schematic representation of fabricating RGrO-and-copper artificial nacre. (a) Ordered porous structure in natural fir wood. (b) Replicating the porous structure of fir wood with Cu. (c) Hot-pressing porous Cu preform absorbed with RGrO. (d) RGrO-and-Copper nacre consisting of RGrO "brick" and copper "mortar".

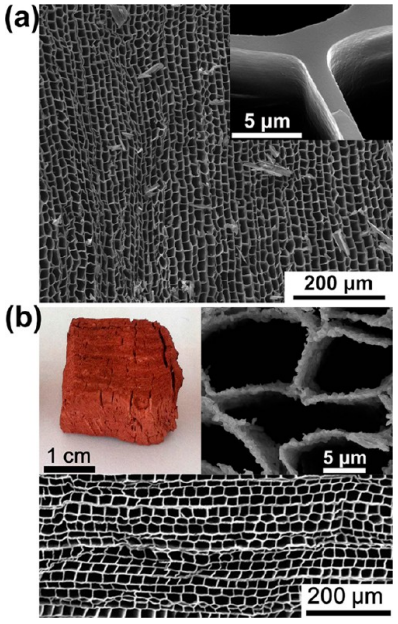

Figure 2. (a) Layered porous structure of fir wood (the wood was carbonized for SEM observation). (b) Monolithic fir-templated porous Cu preform with a typical size of 2 × 1.5 × 1.5 cm^3. High and low magnification SEM images indicate a good replication of the microstructure of fir wood.

To obtain RGrO reinforced metals with a "brick-and-mortar" structure, a greater challenge that not only homogeneous dispersion but also alignment of RGrO in metal matrix has to be surmounted. Here, we have realized homogeneous dispersion as well as ordered alignment of RGrO in Cu by impregnating the ordered porous Cu preform with RGrO solution. RGrO was then absorbed onto the wall of pores after air drying. RGrO was dispersed in Cu matrix very homogeneously because the wall thickness of pores was in submicrometer scale. Moreover, the absorbed RGrO on the wall was aligned in copper matrix because of the highly ordered pores. Finally, nacre-inspired RGrO reinforced Cu matrix composite was obtained by compacting the porous Cu preform with absorbed RGrO. The as-obtained composites are referred to as RGrO-and-Cu nacre.

Graphene oxide (GrO) used here was prepared by a modified Hummers' method.[29] The as-obtained GrO was analyzed by atomic force microscopy (AFM) and Raman spectroscopy. The AFM results (Figure 3a,b) show the GrO with lateral dimensions ranging from ~200 nm to ~2 μm, and a thickness of ~0.94 nm indicates that monolayer was achieved. Raman spectroscopy was used to characterize the structural quality of GrO and RGrO (Figure 3c). The intensity ratio of the D band to the G band I_D/I_G is a measure of defect density for graphene. The obtained GrO with I_D/I_G ratios of 1 has the same quality with that reported in reference.[29] After absorbed into the porous Cu preform, GrO was reduced at elevated temperatures in a mixed atmosphere of hydrogen and argon. The existence and quality of RGrO in the RGrO-and-Cu nacre was also characterized by Raman spectroscopy (Figure 3c). The fraction of RGrO in the RGrO-and-Cu nacres was controlled by changing the concentration of RGrO solution for impregnating. For a given RGrO concentration, the amount of impregnated RGrO was estimated from the porosity of the Cu preform by measuring the macro size and weight of the Cu preform. In detail, for 1 mg mL^{-1} RGrO solution and per unit volume of Cu preform with a porosity of 96%, the impregnated amount of RGrO was 0.96 mg and the weight of Cu was 360 mg (~4% of theoretical density of Cu 8.9 g cm^{-3}), and the fraction of RGrO in final RGrO-and-Cu nacre was calculated to be ~0.3 wt % or ~1.2 vol % (by assuming that the density of RGrO is 1.9 g cm^{-3}).

Comparison of Microstructures. Figure 4a,b shows scanning electron microscope (SEM) images of fracture surface for the pure Cu specimen prepared by

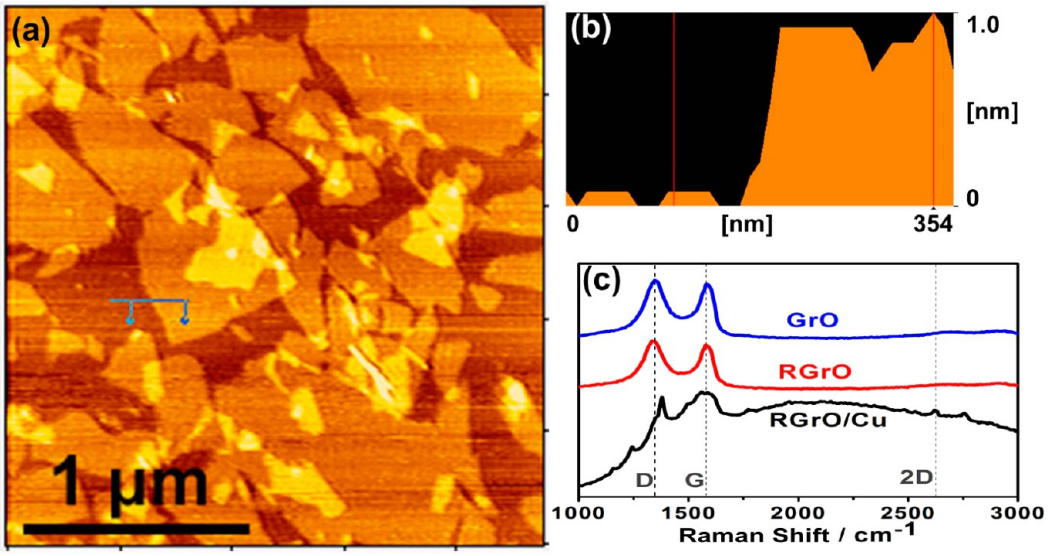

Figure 3. (a,b) AFM image of the GrO prepared by the modified Hummers' method. (c) Raman spectra of the GrO and the RGrO in 1.2 vol % RGrO-and-Cu nacre. That of the pure RGrO reduced by H_2 is also shown for comparison.

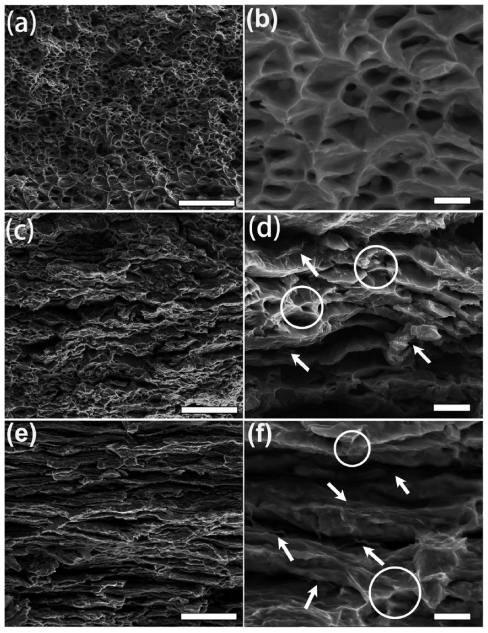

Figure 4. Fracture surface of (a,b) pure copper, (c,d) 0.3 vol % RGrO-and-Cu nacre, and (e,f) 1.2 vol % RGrO-and-Cu nacre with low magnification in the left column and high magnification in the right column. Scale bar: (a,c,e) 30 μm; (b,d,f) 3 μm. The white arrows illustrate the location of RGrO on the fracture surface, and white circles indicate typical ductile fracture area of copper "mortar".

hot-pressing the porous Cu preform. The specimen shows a typical ductile fracture with high plastic deformation consisting of well-developed dimples over the entire surface, which is consistent with that of a normal pure copper. Because of grain growth during hot-pressed compacting, no layered structure or other features inherited from the preform was found in the pure Cu specimen.

RGrO-and-Cu nacres exhibit different microstructure from the pure Cu, in which "brick-and-mortar" organized structures were formed. The expected uniform dispersion and alignment of 2-D RGrO were achieved in the continuous Cu matrix. Figure 4c,d shows the SEM images of fracture surface for the 0.3 vol % RGrO-and-Cu nacre. Figure 4c is the SEM image with a low magnification showing a connected layer microstructure. The SEM image with a higher magnification (Figure 4d) indicates homogeneous dispersion of RGrO throughout the composite without agglomeration (some are pointed out by the small white arrows directly labeled on the image). It also shows that the microstructure of composite inherits the feature of the ordered porous Cu preform; the layers are connected to each other and staggered slits where RGrO locates lay in parallel between them. The microstructure of RGrO-and-Cu organized in the "brick-and-mortar" structure is schematically represented in Figure 1d. The RGrO is surrounded and bonded by Cu matrix, and the continuous matrix exhibits typical behavior of ductile fracture in metals as observed at the edges of layers and some areas pointed out by the white circles directly labeled on the image. Figure 4e,f shows the SEM images of fracture surface for the 1.2 vol % RGrO-and-Cu nacre. Because of higher fraction of RGrO, the layered microstructure is more apparent (Figure 4e), and the RGrO is also homogeneously dispersed throughout the composite without agglomeration (Figure 4f). Ductile fracture of Cu matrix is also observed in this specimen as that in the 0.3 vol % RGrO-and-Cu nacre.

The microstructures were also investigated by using transmission electron microscope (TEM) (Figure 5). The unreinforced copper matrix has a microstructure consisting of equiaxed grains with an average size of 1.0 ± 0.4 μm, and a typical area is shown in Figure 5a. As consistent with SEM images, lamellar boundaries

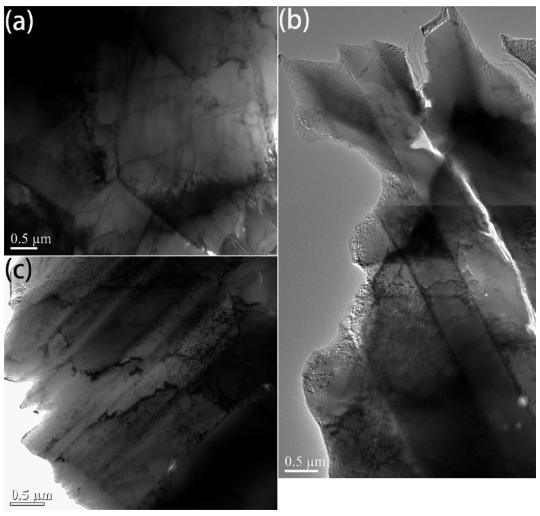

Figure 5. TEM images of (a) unreinforced copper matrix, (b) 0.3 vol % RGrO-and-Cu nacre, and (c) 1.2 vol % RGrO-and-Cu nacre, showing equiaxed grain in unreinforced copper matrix and lamellar structure in RGrO-and-Cu artificial nacres.

were formed in the RGrO reinforced composites. As shown in Figure 5b,c, the thicknesses of lamellae in 0.3 and 1.2 vol % RGrO-and-Cu nacres are in the similar scale, being around 1.0 μm, which is close to that of the wall in porous Cu preform. But the grain size along the lamellae is remarkably larger, indicating the suppression of grain coarsening by RGrO. The interfacial area in 1.2 vol % RGrO-and-Cu nacre (Figure 5c) seems more visible than that in 0.3 vol % RGrO-and-Cu nacre (Figure 5b), which could be caused by the difference on graphene fraction between them.

Mechanical Properties. Mechanical properties of the RGrO-and-Cu nacres were investigated by tensile testing. The tensile stress−strain curves are plotted in Figure 6a. The yield strength of the 1.2 vol % RGrO-and-Cu nacre ($\approx 233 \pm 15$ MPa) was about 120% greater than that of unreinforced Cu matrix ($\approx 106 \pm 10$ MPa) prepared with the same processing route. Tensile strength and Young modulus of the sample increased by ≈41% (from 218 ± 10 to 308 ± 10 MPa) and by ≈12% (from 97 ± 4 to 109 ± 4 GPa), respectively. The combination of increased strength and ductility is another attractive advantage of the RGrO-and-Cu nacres when compared with conventional MMCs. Fracture energy and toughness can be roughly estimated based on the area under the stress−strain curves, indicating that the energy required to fracture the RGrO-and-Cu nacre is 1.4 times (for the case of 0.3 vol % RGrO) and 1.8 times (for 1.2 vol % RGrO) higher than that needed to rupture the pure Cu matrix prepared by the same route. Figure 6b shows strengthening effect of various reinforcements as a function of their volume fractions in Cu matrix composites. The strengthening efficiency R of reinforcement can be expressed as

$$R = (\sigma_c - \sigma_m)/V_r\sigma_m \quad (1)$$

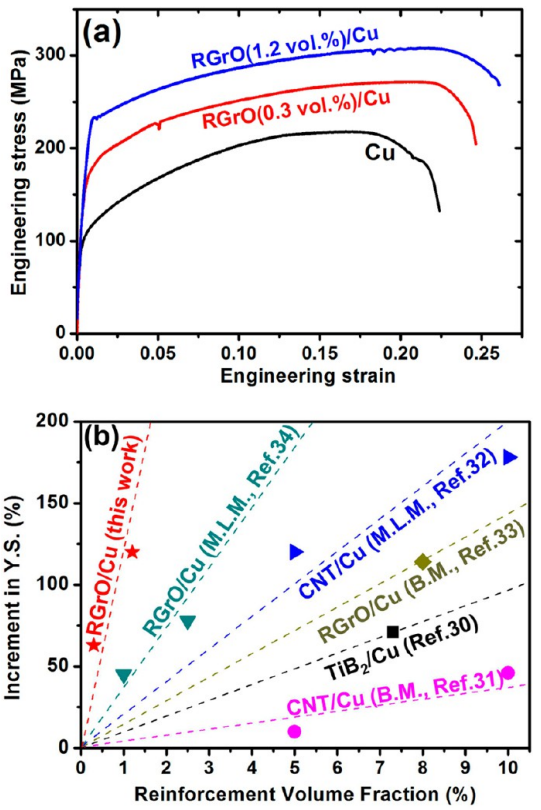

Figure 6. (a) Tensile stress−strain curves of the RGrO-and-Cu nacres, and (b) Strengthening efficiency of various reinforments in Cu matrix composites. Ordinate is the increment in percentage of yield strength; B.M.: ball-milling process; M.L.M.: molecular level mixing process.

where σ_c is the yield strength of the composite, σ_m is the yield strength of the matrix, and V_r is the volume fraction of the reinforcement. The R value of RGrO in RGrO-and-Cu nacres varies from 100 to 210, which is almost 2 orders of magnitude in maximum higher than that of ceramic or carbon nanotube reinforced Cu matrix composites. The superior R of RGrO over ceramic particle[30] and 1-D nanotube[31,32] is related to its high specific surface area and rigid 2-D geometry. Another interesting observation worth to be noted is that the R value in the RGrO-and-Cu nacre is also obviously higher than that of other reported RGrO reinforced Cu matrix composites, such as those prepared by ball milling[33] and even by molecular level mixing,[34] which could be attributed to less structural damage on graphene than ball milling and alignment of RGrO in the "brick-and-mortar" structure. The unidirectionally distributed RGrO in RGrO-and-Cu nacre along the stress is more beneficial to stress transfer than the composites containing randomly oriented RGrO, as predicted by many theoretical models such as the well-established Halpin−Tsai model.[35]

Strengthening and Toughening Mechanisms. The strengthening effect of graphene in metal has been reported in various metal matrices including Mg,[36] Fe,[37] Al,[27,38−43] Ni,[44,45] Cu[34,45−50] and Ti.[51] The key strengthening mechanisms of graphene reported in

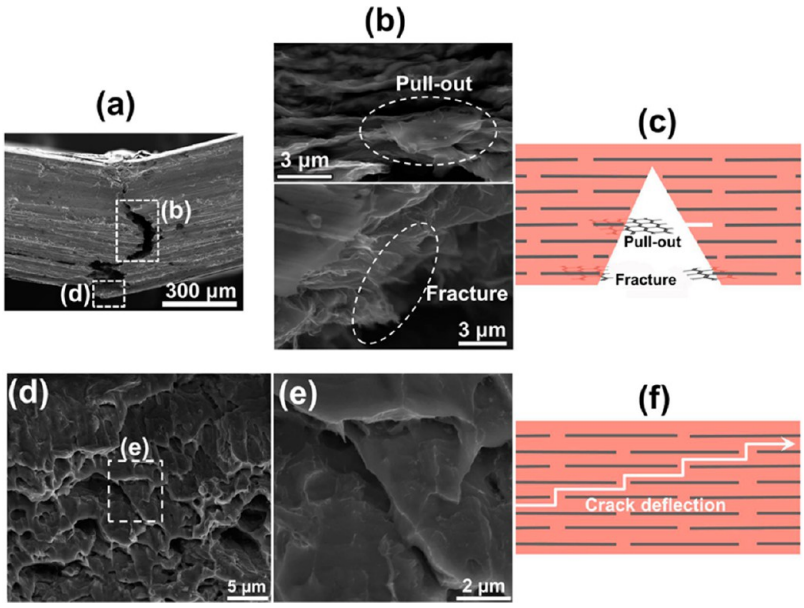

Figure 7. (a) The specimen of 1.2 vol % RGrO-and-Cu nacre after fracture. (b) RGrO pull-out (with smooth edge) and fracture (with torn edge) modes observed at fractured surface. (c) Schematic representation of failure modes of the RGrO. (d) Stepwise fracture parallel to the layers indicating an effective deflection of crack propagating along the RGrO-Cu interface and (e) enlargement of the box marked in image (d). (f) Schematic presentation for crack deflection.

MMCs can be summarized as follows: dislocation strengthening, stress transfer and grain refinement in metal matrices.[52] First of all, as observed by experiments[45] and confirmed by computer simulations,[53] graphene can provide an effective barrier to dislocation motion being the dominant deformation mode in metals, which most probably causes the dominant contribution to their strengthening in reported graphene-metal composites.[27,33−50] Second, stress transfer is another important strengthening mechanism in graphene reinforced MMCs. Both superior mechanical properties (high tensile strength and Young modulus) and unique geometric factors (large aspect ratio, large lateral size and, in turn, large interfacial contact area in composites)[38−41,48,50,51] of graphene are beneficial for transferring stress developed in metal matrix to graphene, but which is sensitive to the interfacial strength between graphene and metal. The efficiency of stress transfer from matrix to graphene could be guaranteed by avoiding severe interfacial reaction,[22] modifying interface by another metal[42,48,50] and possible oxygen mediated chemical bonding between RGrO and metal matrix.[34] Third, refinement of grain size by graphene can also significantly contribute to strengthening of MMCs.[40,42,49] Graphene often wrap around grains at grain boundaries, and grain boundary migration is hampered with high enough volume fraction of graphene in MMCs, which can hinder grain growth during processing and deformation, even being annealed at elevated temperature.[46]

It is reasonable to believe that graphene can toughen composite by impeding crack advance through a crack-tip-shielding mechanism because of its high aspect ratio and large contact area with matrix.[40,51] In ceramic composites, graphene sheet pulling-out from matrix proved to be an effective mechanism for toughening because of energy dissipation contributed by interface debonding and subsequent friction.[54,55] However, those reported graphene reinforced MMCs up to now still mainly focused on the uniform dispersion of graphene and its strengthening effect, while its toughening effect on metal was rarely reported. As far as we know, in accessible literatures, the only result on enhancing strength without losing ductility of metal was reported in graphene nanoflakes reinforced aluminum alloy matrix composites prepared by ball milling and followed hot-pressed compacting.[38] The authors surmised that the performance was probably contributed by the straightening of multiply wrinkled graphene.

To investigate possible toughening mechanisms in RGrO-and-Cu nacres here, fractography analysis was carried out (Figure 7). Figure 7a is the SEM image of the specimen of 1.2 vol % RGrO-and-Cu nacre after fracture. Figure 7b depicts the morphology of RGrO at the fracture surface, from which possible failure mode of RGrO during fracturing the composites could be disclosed. A simple shear lag model has been successfully applied to explain the strength and toughness of nacre, according to which the applied load is transferred to "bricks" through shear stresses developed in "mortar". The strengthening and toughening efficiencies of "brick" in nacre-inspired composites depend on its operative failure mode; "brick" exerts its maximum strength and fragile rupture emerges and thus composite is strong but brittle when breaking under a

"brick" fracture mode, whereas maximum strength of "brick" is not achieved but more energy are dissipated by interface debonding and subsequent friction and thus composites are relatively weak but ductile when rupturing under a "brick" pull-out mode. In the simple shear lag model, the critical aspect ratio (s_c) that determines the above two operative failure modes is equal to the ratio of σ_p/τ_y, where σ_p is the tensile strength of "brick" and τ_y the yield shear strength of "mortar". The composite fails under the "brick" fracture mode for actual aspect ratio (s) of "brick" larger than the critical value ($s > s_c$), while under the "brick" pull-out mode in the case of $s < s_c$. The Young's modulus and fracture strength of defect-free graphene was measured by an AFM indentation method as 1.0 TPa and 130 GPa, respectively.[56] By a similar measure method, RGrO exhibited a smaller elastic modulus with a mean value of 0.25 (±0.15) TPa.[57] Therefore, the tensile strength of RGrO could be estimated on the scale of tens of GPa although it was not measured. On the other hand, the shear strength of Cu is in the range of 150−230 MPa. The critical aspect ratio s_c is thereby estimated to be hundreds for RGrO reinforced MMC. The actual aspect ratio of RGrO prepared here, with a thickness of <1 nm and varied lateral sizes ranging from hundreds of nanometers to several micrometers as indicated by AFM, covered the calculated critical aspect ratio s_c. This wide range of actual aspect ratio implied that a possible combined failure mode took effect in the RGrO-and-Cu nacres investigated (Figure 7c); RGrO with small aspect ratio ($s < s_c$) mainly contributed to toughness through a pull-out mode, while that with large aspect ratio ($s > s_c$) mainly contributed to strength through a fracture mode. This conjecture could be supported by different edge morphologies of RGrO at fracture surface, torn edge for the fragile fracture mode and smooth edge for the pulling-out mode (Figure 7b). Although some positive results have been achieved on the bioinspired strategy here, the actual aspect ratio of RGrO need be restricted in a narrower distribution range, below or above the calculated critical value s_c in different composites, to compare and verify whether the combined failure mode is more efficient than the individual one for strengthening-toughening metal or not.

Another important toughening mechanism may be related to the energy dissipation caused by the process of crack deflection, during which an initial crack tilts and twists and is forced to move out of the initial propagation plane when it encounters a rigid reinforcement.[58] Such deflection causes a change in the stress state from mode I (tensile/opening) to mixed-mode I/II (tensile/in-plane shear) in the case that the crack tilts, or mix-mode I/III (tensile/antiplane shear) if the crack twists. Crack propagation under mixed mode conditions requires a higher driving force than in mode I, which results in higher fracture toughness of the composites.[58] The critical energy release rate G_{Ic}, an energy criterion for crack propagation, is related to the area of net generated fracture surface. The deflection processes increase the total fracture surface area, resulting in greater energy absorption as compared to an unfilled matrix. Increase in fracture toughness contributed by the process of crack deflection has been certified in both natural nacre and artificial composites with a "brick-and-mortar" structure.[5,7,19,59] In order to verify this effect in our RGrO-and-Cu artificial nacres, a fractography analysis was carried out. Representative SEM fracture micrographs are depicted in Figure 7d−f. The fractured surface revealed a typical stepwise fracture observed parallel to layers (Figure 7d−f), and some RGrO fragments were also observed on the fractured steps, indicating that the staggered RGrO had played a role in hindering and/or deviating crack. Crack deflection processes may be highly effective for RGrO given its 2-D geometry and large aspect ratio,[60] especially in the case of our RGrO-and-Cu artificial nacres with aligned RGrO.

Strong interfacial strength between reinforcement and matrix ensures high load-transfer efficiency in composites. In a composite, the interfacial strength is decided by many factors, such as processing route, interfacial reaction and bonding. High resolution TEM is used to study the interface between graphene and the copper matrix. Figure 8a is a representative high resolution TEM image, showing that the interfaces are free of impurities, voids, or gaps. It is no easy to reveal the interface structure with single or double graphene layer because of an extremely thin thickness. To characterize the quality of the interface clearly, an interfacial area marked in Figure 8a containing multilayered graphene with an interplanar distance of 0.34 nm was presented in Figure 8b. As we can see, the graphene and the copper have clear and strong interfaces which are bonding in atomic scale. Precise value of adhesion energy between reinforcement and matrix is a tough task, but recently the adhesion energy between graphene and Cu were measured by using a double cantilever beam (DCB) test. The results indicated that the adhesion energy value for graphene and Cu matrix in sintered graphene/Cu composite was about 200 times higher than that for graphene as-grown on Cu substrate by the chemical vapor deposition (CVD) method.[34,61] On the other hand, the adhesion of RGrO on Cu can also be promoted by the chemical bonds induced by residual intermediate oxygen between RGrO and Cu in RGrO/Cu composite.[34] In this work, comparably high adhesion energy could be expected in the RGrO-and-Cu nacres because residual oxygen of RGrO and hot-pressed compacting can promote the formation of chemical bonds. Figure 8c shows the TEM images of layered Cu matrix and fractured interfaces. Equiaxed Cu grains with a size of 500−1500 nm were

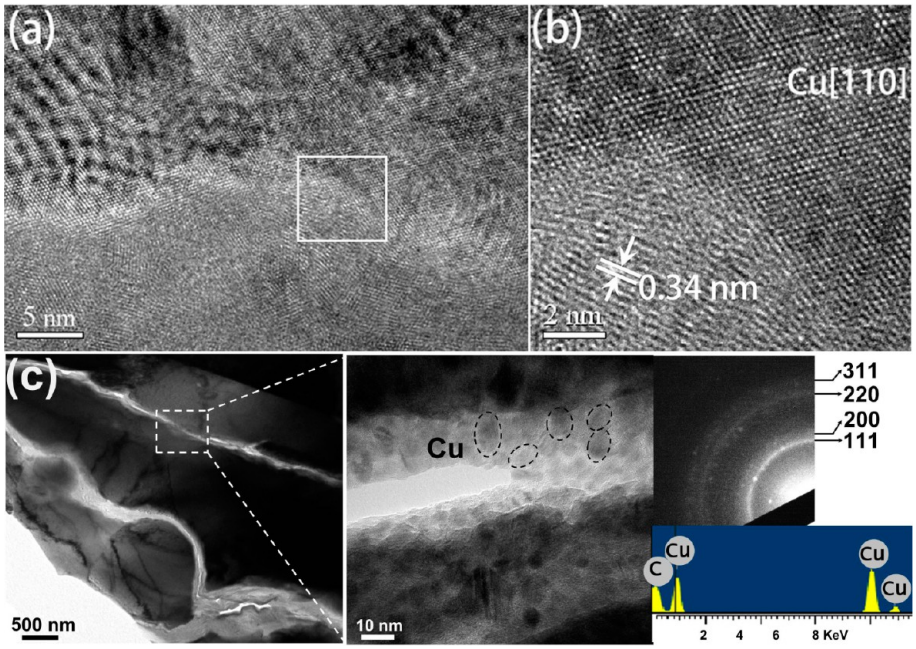

Figure 8. (a) Typical interfacial structure in the specimen of 1.2 vol % RGrO-and-Cu nacre. (b) Area marked in (a) with higher magnification, and clear interface between graphene and Cu can be observed. (c) TEM analysis for 1.2 vol % RGrO-and-Cu nacre after fracture. Copper nanoparticles were observed on delaminated RGrO, indicating good interfacial bonding between RGrO and copper matrix.

found in the matrix and the grains across the layers. Magnified TEM image of failure interface indicates that Cu nanoparticles exist on the surface of delaminated RGrO, illustrating strong interfacial bonding between RGrO and Cu matrix in the RGrO-and-Cu nacres.

Evaluation on Electrical Conductivity. Compositing may also compromise other properties of metals, such as conductivity, but the electrical conductivities of the RGrO-and-Cu nacres are very close to that of a standard annealed copper conductor, 57.5×10^6 S m^{-1} of International Annealed Copper Standard (IACS). The electrical conductivity was evaluated by the eddy current method. The conductivity of the pure Cu in this work was measured to be $55.3(0.2) \times 10^6$ S m^{-1}, 0.3 vol % RGrO-and-Cu nacre to be $54.4(0.2) \times 10^6$ S m^{-1}, and 1.2 vol % RGrO-and-Cu nacre to be $56.6(0.2) \times 10^6$ S m^{-1}, which is obviously higher than that of graphene-copper composites prepared by molecular level mixing[34] and electrochemical deposition.[46] The high electrical conductivity of the RGrO-and-Cu nacres might be attributed to the continuous pathway for electrons transport provided by the uninterrupted Cu "mortar".

CONCLUSION

In summary, we demonstrated successful fabrication of nanostructured RGrO-and-Cu artificial nacre by a preform impregnation process, inserting RGrO "bricks" into fir wood-templated layered porous Cu preform (acts as "mortar" after compacting), by which uniform dispersion and alignment of RGrO in Cu was achieved. This preform impregnation process potentially paves a new path for fabricating other nacre-inspired composites because of its advantage of uniform dispersion and alignment of reinforcement in matrix in one-step, especially for those composites with remarkably different physical and chemical properties between reinforcement and matrix. The measured mechanical properties showed simultaneous enhancement on strength and ductility by introducing the nacre-inspired "brick-and-mortar" structure in MMC and high strengthening efficiency of aligned 2-D RGrO. Bioinspired strategy shed light on how to solve the conflict between strength and toughness in MMCs.

METHODS

Porous Cu Preform Preparation. The specimens (~35 × 25 × 15 mm^3) of fir wood were boiled in 5% dilute ammonia for 6 h to get rid of gums and fatty acids inside and enhance the pore connectivity for the precursor. The extracted fir wood templates were washed by deionized water and freeze-dried to prevent the collapse of porous. The copper ions precursor solution was prepared by analytically pure copper nitrate $Cu(NO_3)_2 \cdot 3H_2O$, ethanol and deionized water with the ratio of 120 mmol:50 mL:50 mL. Then the fir wood templates were vacuumed in sealed flask at first and then impregnated with the injected copper ions precursor solution at 60 °C for 24 h. The samples were taken out from the solution and then air-dried at 60 °C for 12 h. Finally, the samples were heated up to 900 °C with a heating rate of 30 °C/h

and maintained at the same temperature for another 2 h in air. Porous Cu preforms were then obtained by reducing the specimens in a mixed atmosphere of 20 vol % H_2/Ar at 450 °C for 3 h.

Graphene Oxide Preparation. Graphene oxide was prepared based on a modified Hummers route.[29] The obtained graphite oxide was purified by repeated centrifugation and dispersion in cold water until the pH of the supernatant was neutral. Finally, graphene oxide was yielded by sonication (2 h under power of 480 W) using a bath sonicator.

RGrO-and-Copper Nacre Preparation. The as-prepared porous Cu preforms were impregnated with the as-obtained graphene oxide solution above. Fraction of graphene oxide in final composite was controlled by varying the concentration of solution at this step. The impregnated Cu preforms were dried in air-dry oven at 30 °C, and then heated up to 450 °C in 3 h and maintained at the same temperature for another 3 h under a 20 vol % H_2/Ar mixed atmosphere. The as-obtained porous RGrO-Cu preforms were then consolidated at an applied pressure of 50 MPa and temperature of 950 °C for 10 min under an Ar atmosphere. To obtain "brick-and-mortar" structure as ordered as possible, the pressure was applied perpendicular to the layer (as shown in Figure 1c).

Characterization. The morphology and structure of GrO were characterized by AFM ("E-Sweep" of the NanoNavi-Series) and Raman spectroscopy (Senterra R200-L, Bruker). The microstructures of the porous Cu preform and the RGrO-and-Cu nacre were observed by SEM (FEI SIRION 200) and TEM (JEOL JEM-2100F). For tensile testing, the obtained samples were cut using a wire electrical discharging machine and were polished to a dog-bone shape with gauge length of 8 mm and gauge width of 2 mm. The tensile testing was conducted with a crosshead speed of 0.6 mm/min at room temperature.

Conflict of Interest: The authors declare no competing financial interest.

Acknowledgment. The authors would like to acknowledge the financial support from the Natural Science Foundation of China (Nos.51371115, 51131004, 51071100), the Ministry of Science & Technology of China (973 program) (No.2012CB619600), Shanghai Science & Technology Committee (Nos.14JC1403300, 14DZ2261200).

REFERENCES AND NOTES

1. Mortensen, A.; Llorca, J. Metal Matrix Composites. *Annu. Rev. Mater. Res.* **2010**, *40*, 243–270.
2. Miracle, D. B. Metal Matrix Composites—From Science to Technological Significance. *Compos. Sci. Technol.* **2005**, *65*, 2526–2540.
3. Tiong, C. S. Novel Nanoparticle-Reinforced Metal Matrix Composites with Enhanced Mechanical Properties. *Adv. Eng. Mater.* **2007**, *9*, 639–652.
4. Zhao, Y.-H.; Liao, X.-Z.; Cheng, S.; Ma, E.; Zhu, Y. T. Simultaneously Increasing the Ductility and Strength of Nanostructured Alloys. *Adv. Mater.* **2006**, *18*, 2280–2283.
5. Ritchie, R. O. The Conflicts between Strength and Toughness. *Nat. Mater.* **2011**, *10*, 817–822.
6. Miserez, A.; Müller, R.; Mortensen, A. Increasing the Strength/Toughness Combination of High Volume Fraction Particulate Metal Matrix Composites Using an Al-Ag Matrix Alloy. *Adv. Eng. Mater.* **2006**, *8*, 56–62.
7. Wegst, U. G. K.; Bai, H.; Saiz, E.; Tomisa, A. P.; Ritchie, R. O. Bioinspired Structural Materials. *Nat. Mater.* **2015**, *14*, 23–36.
8. Meyers, M. A.; McKittrick, J.; Chen, P.-Y. Structural Biological Materials: Critical Mechanics-Materials Connections. *Science* **2013**, *339*, 773–779.
9. Yao, H.-B.; Ge, J.; Mao, L.-B.; Yan, Y.-X.; Yu, S.-H. 25th Anniversary Article: Artificial Carbonate Nanocrystals and Layered Structural Nanocomposites Inspired by Nacre: Synthesis, Fabrication and Applications. *Adv. Mater.* **2014**, *26*, 163–188.
10. Cheng, Q. F.; Jiang, L.; Tang, Z. Y. Bioinspired Layered Materials with Superior Mechanical Performance. *Acc. Chem. Res.* **2014**, *47*, 156–1266.
11. Novoselov, K. S.; Fal'ko, V. I.; Colombo, I.; Gellert, P. R.; Schwab, M. G.; Kim, K. A Roadmap for Graphene. *Nature* **2012**, *490*, 192–200.
12. Cui, W.; Li, M. Z.; Liu, J. Y.; Wang, B.; Zhang, C.; Jiang, L.; Cheng, Q. F. A Strong Integrated Strength and Toughness Artificial Nacre Based on Dopamine Cross-Linked Graphene Oxide. *ACS Nano* **2014**, *8*, 9511–9517.
13. Hu, K. S.; Gupta, M. K.; Kulkarni, D. D.; Tsukruk, V. V. Ultra-Robust Graphene Oxide-Silk Fibroin Nanocomposite Membranes. *Adv. Mater.* **2013**, *25*, 2301–2307.
14. Cheng, Q. F.; Wu, M. X.; Li, M. Z.; Jiang, L.; Tang, Z. Y. Ultratough Artificial Nacre Based on Conjugated Cross-linked Graphene Oxide. *Angew. Chem., Int. Ed.* **2013**, *52*, 3750–3755.
15. Corni, I.; Harvey, T. J.; Wharton, J. A.; Stokes, K. R.; Walsh, F. C.; Wood, R. J. K. A Review of Experimental Techniques to Produce a Nacre-like Structure. *Bioinspiration Biomimetics* **2012**, *7*, 031001.
16. Bonderer, L. J.; Studart, A. R.; Gauckler, L. J. Bioinspired Design and Assembly of Platelet Reinforced Polymer Films. *Science* **2008**, *319*, 1069–1073.
17. Podsiadlo, P.; Kaushik, A. K.; Arruda, E. M.; Waas, A. M.; Shim, B. S.; Xu, J. D.; Nandivada, H.; Pumplin, B. G.; Lahann, J.; Ramamoorthy, A.; *et al.* Ultrastrong and Stiff Layered Polymer Nanocomposites. *Science* **2007**, *318*, 80–83.
18. Tang, Z. Y.; Kotov, N. A.; Magonov, S.; Ozturk, B. Nanostructured Artificial Nacre. *Nat. Mater.* **2003**, *2*, 413–418.
19. Munch, E.; Launey, M. E.; Alsem, D. H.; Saiz, E.; Tomsia, A. P.; Ritchie, R. O. Tough, Bio-Inspired Hybrid Materials. *Science* **2008**, *322*, 516–520.
20. Long, B.; Wang, C. A.; Lin, W.; Huang, Y.; Sun, J. L. Polyacrylamide-Clay Nacre-Like Nanocomposites Prepared by Electrophoretic Deposition. *Compos. Sci. Technol.* **2007**, *67*, 2770–2774.
21. Yao, H. B.; Tan, Z. H.; Fang, H. Y.; Yu, S. H. Artificial Nacre-like Bionanocomposite Films from the Self-Assembly of Chitosan-Montmorillonite Hybrid Building Blocks. *Angew. Chem., Int. Ed.* **2010**, *49*, 10127–10131.
22. Bartolucci, S. F.; Paras, J.; Rafiee, M. A.; Rafiee, J.; Lee, S.; Kapoor, D.; Koratkar, N. Graphene-Aluminum Nanocomposites. *Mater. Sci. Eng., A* **2011**, *528*, 7933–7937.
23. Deng, X.; Chawla, N.; Chawla, K. K.; Koopman, M.; Chu, J. P. Mechanical Behavior of Multilayered Nanoscale Metal-Ceramic Composites. *Adv. Eng. Mater.* **2005**, *7*, 1099–1108.
24. Deville, S.; Saiz, E.; Nalla, R. K.; Tomsia, A. P. Freezing as a Path to Build Complex Composites. *Science* **2006**, *311*, 515–518.
25. Jiang, L.; Li, Z. Q.; Fan, G. L.; Zhang, D. A Flake Powder Metallurgy Approach to Al_2O_3/Al Biomimetic Nanolaminated Composites with Enhanced Ductility. *Scr. Mater.* **2011**, *65*, 412–415.
26. Jiang, L.; Li, Z. Q.; Fan, G. L.; Cao, L. L.; Zhang, D. Strong and Ductile Carbon Nanotube(CNT)/Aluminum Bulk Nanolaminated Composites with Two-Dimensional Alignment of CNTs. *Scr. Mater.* **2012**, *66*, 331–334.
27. Wang, J. Y.; Li, Z. Q.; Fan, G. L.; Pan, H. H.; Chen, Z. X.; Zhang, D. Reinforcement with Graphene Nanosheets in Aluminum Matrix Composites. *Scr. Mater.* **2012**, *66*, 594–597.
28. Li, Z.; Fan, G. L.; Tan, Z. Q.; Guo, Q.; Xiong, D.-B.; Su, Y. S.; Li, Z. Q.; Zhang, D. Uniform Dispersion of Graphene Oxide in Aluminum Powder by Direct Electrostatic Adsorption for Fabrication of Graphene/Aluminum Composites. *Nanotechnology* **2014**, *25*, 325601.
29. Eigler, S.; Enzelberger-Heim, M.; Grimm, S.; Hofmann, P.; Kroener, W.; Geworski, A.; Dotzer, C.; Röckert, M.; Xiao, J.; Papp, C.; *et al.* Wet Chemical Synthesis of Graphene. *Adv. Mater.* **2013**, *25*, 3583–3587.
30. Tu, J. P.; Wang, N. Y.; Yang, Y. Z.; Qi, W. X.; Liu, F.; Zhang, X. B.; Lu, H. M.; Liu, M. S. Preparation and Properties of TiB_2 Nanoparticle Reinforced Copper Matrix Composites by *In Situ* Processing. *Mater. Lett.* **2002**, *52*, 448–452.
31. Kim, K. D.; Cha, S. I.; Hong, S. H.; Hong, S. H. Microstructures and Tensile Behavior of Carbon Nanotube Reinforced Cu Matrix Nanocomposites. *Mater. Sci. Eng., A* **2006**, *430*, 27–33.

32. Cha, S. I.; Kim, K. T.; Arshad, S. N.; Mo, C. B.; Hong, S. H. Extraordinary Strengthening Effect of Carbon Nanotube in Metal-Matrix Nanocomposites Processed by Molecular-Level Mixing. *Adv. Mater.* **2005**, *17*, 1377–1381.
33. Chu, K.; Jia, C. C. Enhanced Strength in Bulk Graphene-Copper Composites. *Phys. Status Solidi A* **2014**, *211*, 184–190.
34. Hwang, J.; Yoon, T.; Jin, S. H.; Lee, J.; Kim, T.-S.; Hong, S. H.; Jeon, S. Enhanced Mechanical Properties of Graphene/Copper Nanocomposites Using a Molecular-Level Mixing Process. *Adv. Mater.* **2013**, *25*, 6724–6729.
35. Halpin, J. C.; Kardos, J. L. The Halpin-Tsai Equations: A Review. *Polym. Eng. Sci.* **1976**, *16*, 344–352.
36. Chen, L.-Y.; Konishi, H.; Fehrenbacher, A.; Ma, C.; Xu, J.-Q.; Choi, H.; Xu, H.-F.; Pfefferkorn, F. E.; Li, X.-C. Novel Nanoprocessing Route for Bulk Graphene Nanoplatelets Reinforced Metal Matrix Nanocomposites. *Scr. Mater.* **2012**, *67*, 29–32.
37. Lin, D.; Liu, C. R.; Cheng, G. J. Single-Layer Graphene Oxide Reinforced Metal Matrix Composites by Laser Sintering: Microstructure and Mechanical Property Enhancement. *Acta Mater.* **2014**, *80*, 183–193.
38. Yan, S. J.; Dai, S. L.; Zhang, X. Y.; Yang, C.; Hong, Q. H.; Chen, J. Z.; Lin, Z. M. Investigating Aluminum Alloy Reinforced by Graphene Nanoflakes. *Mater. Sci. Eng., A* **2014**, *612*, 440–444.
39. Shin, S. E.; Choi, H. J.; Shin, J. H.; Base, D. H. Strengthening Behavior of Few-Layered Graphene/Aluminum Composites. *Carbon* **2015**, *82*, 143–151.
40. Li, J. L.; Xiong, Y. C.; Wang, X. D.; Yan, S. J.; Yang, C.; He, W. W.; Chen, J. Z.; Wang, S. Q.; Zhang, X. Y.; Dai, S. L. Microstructure and Tensile Properties of Bulk Nanostructured Aluminum/Graphene Composites Prepared *via* Cryomilling. *Mater. Sci. Eng., A* **2015**, *626*, 400–405.
41. Zhao, L. Y.; Lu, H. M.; Gao, Z. J. Microstructure and Mechanical Properties of Al/Graphene Composite Produced by High-Pressure Torsion. *Adv. Eng. Mater.* **2014**, 10.1002/adem.201400375.
42. Zhao, Z. Y.; Guan, R. G.; Guan, X. H.; Feng, Z. X.; Chen, H.; Chen, Y. Microstructures and Properties of Graphene-Cu/Al Composite Prepared by a Novel Process Through Clad Forming and Improving Wettability with Copper. *Adv. Eng. Mater.* **2015**, *17*, 663–668.
43. Bastwros, M.; Kim, G.-Y.; Zhu, C.; Zhang, K.; Wang, S. R.; Tang, X. D.; Wang, X. W. Effect of Ball Milling on Graphene Reinforced Al6061 Composite Fabricated by Semi-Solid Sintering. *Compos. Part B* **2014**, *60*, 111–118.
44. Kuang, D.; Xu, L. Y.; Liu, L.; Hu, W. B.; Wu, Y. T. Graphene-Nickel Composites. *Appl. Surf. Sci.* **2013**, *273*, 484–490.
45. Kim, Y.; Lee, J.; Yeom, M. S.; Shin, J. W.; Kim, H.; Cui, Y.; Kysar, J. W.; Hone, J.; Jung, Y.; Jeon, S.; *et al.* Strengthening Effect of Single-Atomic-Layer Graphene in Metal-Graphene Nanolayered Composites. *Nat. Commun.* **2013**, *4*, 2114.
46. Pavithra, C. L. P.; Sarada, B. V.; Rajulapati, K. V.; Rao, T. N.; Sundararajan, G. A New Electrochemical Approach for the Synthesis of Copper-Graphene Nanocomposite Foils with High Hardness. *Sci. Rep.* **2014**, *4*, 4049.
47. Kim, W. J.; Lee, T. J.; Han, S. H. Multi-Layer Graphene/Copper Composites: Preparation Using High-Ratio Differential Speed Rolling, Microstructure and Mechanical Properties. *Carbon* **2014**, *69*, 55–65.
48. Tang, Y. X.; Yang, X. M.; Wang, R. R.; Li, M. X. Enhancement of the Mechanical Properties of Graphene-Copper Composites with Graphene-Nickel Hybrids. *Mater. Sci. Eng., A* **2014**, *599*, 247–254.
49. Chu, K.; Jia, C. C. Enhanced Strength in Bulk Graphene-Copper Composites. *Phys. Status Solidi A* **2014**, *211*, 184–190.
50. Li, M. X.; Che, H. W.; Liu, X. Y.; Liang, S. X.; Xie, H. L. Highly Enhanced Mechanical Properties in Cu Matrix Composites Reinforced with Graphene Decorated Metallic Nanoparticles. *J. Mater. Sci.* **2014**, *49*, 3725–3731.
51. Xu, Z. S.; Shi, X. L.; Zhai, W. Z.; Yao, J.; Song, S. Y.; Zhang, Q. X. Preparation and Tribological Properties of TiAl Matrix Composites Reinforced by Multilayer Graphene. *Carbon* **2014**, *67*, 168–177.
52. Ovid'ko, I. A. Metal-Graphene Nanocomposites with Enhanced Mechanical Properties: A Review. *Rev. Adv. Mater. Sci.* **2014**, *38*, 190–200.
53. Chang, S.-W.; Nair, A. K.; Buehler, M. J. Nanoindentation Study of Size Effects in Nickel-Graphene Nanocomposites. *Philos. Mag. Lett.* **2013**, *93*, 196–203.
54. Walker, L. S.; Marotto, V. R.; Rafiee, M. A.; Koratkar, N.; Corral, E. Toughening in Graphene Ceramic Composite. *ACS Nano* **2011**, *5*, 3182–3190.
55. Lee, B.; Koo, M. Y.; Jin, S. H.; Kim, K. T.; Hong, S. H. Simultaneous Strengthening and Toughening of Reduced Graphene Oxide/Alumina Composites Fabricated by Molecular-Level Mixing Process. *Carbon* **2014**, *78*, 212–219.
56. Lee, C. G.; Wei, X. D.; Kysar, J. W.; Hone, J. Measurement of the Elastic Properties and Intrinsic Strength of Monolayer Graphene. *Science* **2008**, *321*, 385–388.
57. Navarro-Gómez, C.; Burghard, M.; Kern, K. Elastic Properties of Chemically Derived Single Graphene Sheets. *Nano Lett.* **2008**, *8*, 2045–2049.
58. Wetzel, B.; Rosso, P.; Haupert, F.; Friedrich, K. Epoxy Nanocomposites-Fracture and Toughening Mechanisms. *Eng. Fract. Mech.* **2006**, *73*, 2375–2398.
59. Bouville, F.; Maire, E.; Meille, S.; Van de Moortele, B.; Stevenson, A. J.; Deville, S. Strong, Tough and Stiff Bio-inspired Ceramics from Brittle Constituents. *Nat. Mater.* **2014**, *13*, 508–514.
60. Rafiee, M. A.; Rafiee, J.; Wang, Z.; Song, H. H.; Yu, Z. Z.; Koratkar, N. Enhanced Mechanical Properties of Nanocomposites at Low Graphene Content. *ACS Nano* **2009**, *3*, 3884–3890.
61. Yoon, T.; Shin, W. C.; Kim, T. Y.; Mun, J. H.; Kim, T.-S.; Cho, B. J. Direct Measurement of Adhesion Energy of Monolayer Graphene As-Grown on Copper and Its Application to Renewable Transfer Process. *Nano Lett.* **2012**, *12*, 1448–1452.